High-order-harmonic generation using gas-phase H_2O molecules

Song-Feng Zhao,[1,2] Cheng Jin,[1] R. R. Lucchese,[3] Anh-Thu Le,[1] and C. D. Lin[1]

[1]*J. R. Macdonald Laboratory, Department of Physics, Kansas State University, Manhattan, Kansas 66506, USA*

[2]*Key Laboratory of Atomic and Molecular Physics and Functional Materials of Gansu Province,
College of Physics and Electronic Engineering, Northwest Normal University, Lanzhou 730070, China*

[3]*Department of Chemistry, Texas A&M University, College Station, Texas 77843-3255, USA*

We investigate high-order-harmonic generation of isotropically distributed gas-phase H_2O molecules exposed to an intense laser field. The induced dipole of each individual molecule by the laser field is first calculated using the recently developed quantitative rescattering theory. In a thin medium, harmonic spectra generated coherently from all the molecules are then calculated by solving Maxwell's equation of propagation. By using accurate transition dipoles of H_2O, we show that the harmonics in the lower plateau region are quite different from models that employ the simpler strong-field approximation. We also examine the magnitude and phase of the harmonics and their dependence on laser focusing conditions.

I. INTRODUCTION

High-order-harmonic generation (HHG) of atoms and molecules exposed to a strong infrared (IR) laser field has been widely studied in recent years, both experimentally and theoretically [1–4]. The HHG has long been used to generate coherent extreme ultraviolet lights [5,6] as well as attosecond pulses [7–13]. In the last few years, many experiments have reported HHG spectra from molecular targets, and some are from nonlinear polyatomic molecules [14–21]. On the theoretical side, a number of papers have reported calculations of HHG from nonlinear polyatomic molecules as well [22–27]. In these theoretical works, all the calculations have focused only on the response from an individual molecule, while experimental measurements are for HHG from a collection of molecules in the medium. To compare with experimental data, theory has to account for the macroscopic propagation effect [28–30]. However, as far as we know, such calculations have never been done for HHG generated from nonlinear polyatomic molecules.

HHG has been well understood conceptually based on the three-step model [31,32]. Electrons that tunnel through the potential barrier formed by the Coulomb force and the laser field may later be driven back, where they recombine with the ion to emit high-energy photons. For atomic targets, HHG has been studied by solving the time-dependent Schrödinger equation (TDSE) based on the single-active-electron approximation. In principle, one can also investigate HHG from a single molecule by solving multielectron TDSE. However, such calculations are too large and very time-consuming. Attempts have been made only for simple molecules, such as H_2^+ [33–35] and HeH^{2+} [36]. Multielectron molecules in laser fields have been investigated using time-dependent density-functional theory (TDDFT) [37,38]. In addition to these elaborate calculations, simpler models based on strong-field approximation (SFA) [39] have been widely used [24,27,40–45]. The SFA is much easier to calculate than TDSE and TDDFT, but its accuracy is limited, except for explaining some general features, such as the dependence of HHG on the orbital symmetry of the molecule in the ground state and two-center interference effects [33].

An alternative to the theoretical models above is the recently proposed quantitative rescattering (QRS) theory [3,46–48]. At the single atom or single molecule level, the QRS has been used to explain many experimental HHG results [47–52]. The QRS calculated the single-molecule laser-induced dipole moment as the product of a returning electronic wave packet and the accurate photorecombination transition dipole. The latter is obtained by using a state-of-the-art molecular photoionization code [53,54] where the calculations have been widely used to compare photoionization cross sections (PICSs) of molecules measured using synchrotron radiations. The QRS has simplicity similar to the SFA model, but the accuracy is close to calculations based on TDSE or TDDFT, when comparisons are available. Due to its simplicity, the QRS has also now been applied to obtain HHG spectra where a macroscopic propagation effect is included for rare gas atoms [55] under the low-pressure condition and for linear molecules [29,56]. We mention that propagation effects for atomic targets are commonly carried out using single-atom induced dipoles obtained from the SFA-type models [28,57]. In a few cases, induced dipoles obtained from TDSE-type calculations have been reported [30,58]. Outside of our recent works, we are not aware of any investigations of HHG spectra from molecules where macroscopic propagation effects have been considered.

In this paper, we extend the work of Jin *et al.* [29,55,56] to study HHG from nonlinear polyatomic molecules, taking isotropically distributed gas-phase H_2O as examples. We show that calculations of induced dipoles for single molecules using the QRS is actually even simpler than those from using the standard SFA, particularly for molecules that are not oriented. We also show how the QRS theory is applied to H_2O molecules and how the HHG spectra look after propagation in the medium. The major effect of macroscopic propagation is to clean up the spectra and sharpen the odd harmonics that result from phase matching of harmonics in the medium. However, the phase-matching condition depends on many factors in the experiment. We mention that HHG spectra from gaseous H_2O molecules have been reported in [21]. Unfortunately, these measurements were carried out near the saturation intensity,

while the present calculations are limited to lower intensities where the medium is not severely ionized. When medium ionization is large, the fundamental fields are modified during the propagation. To simulate such modifications, the dispersion and absorption coefficients and the Kerr coefficients of H_2O are needed, but they are not all available over the spectral region considered.

II. THEORETICAL METHODS

The theory part is separated into two sections. We first describe the propagation theory used in this work for harmonics generated in a macroscopic medium. And then we discuss how to generate laser-induced dipoles for single nonlinear molecules. For the latter we briefly describe the often-used SFA and the QRS theory. Based on the QRS, we show that it is also possible to simplify the standard SFA model, which is called the factorized SFA model. The factorized SFA can be conveniently used to study qualitative behavior of HHG generated from polyatomic molecules, as will be shown later.

A. Propagation equations

In the present simulation, the fundamental IR field is taken to be a Gaussian beam in space. For the harmonic fields, we assume that absorption and free-electron dispersion can be neglected. These approximations limit us to experiments carried out at low laser intensity and low gas pressure. Under these conditions, the propagation equation of the harmonic field is given by [28,55]

$$\nabla_\perp^2 \widetilde{E}_h(r,z',\omega) - \frac{2i\omega}{c}\frac{\partial \widetilde{E}_h(r,z',\omega)}{\partial z'} = -\mu_0\omega^2 \widetilde{P}_{nl}(r,z',\omega),$$
(1)

where

$$\widetilde{E}_h(r,z',\omega) = \widehat{F}[E_h(r,z',t')],$$
(2)

$$\widetilde{P}_{nl}(r,z',\omega) = \widehat{F}[\overline{P}_{nl}(r,z',t'')]e^{-i(\omega/\omega_0)\varphi_{laser}(r,z')}.$$
(3)

Here $\widehat{F}$ is the Fourier transform operator acting on the temporal coordinate, and ω_0 is the central frequency of the IR laser, $\varphi_{laser}(r,z')$ is the geometric phase (see Ref. [55]), and $\overline{P}_{nl}(r,z',t'')$ is the orientation-averaged nonlinear polarization for nonlinear polyatomic molecules,

$$\overline{P}_{nl}(r,z',t'') = [n_0 - \overline{n}_e(r,z',t'')]\overline{x}(r,z',t''),$$
(4)

where n_0 is the neutral molecule density, $\overline{n}_e(r,z',t'')$ is the orientation-averaged free-electron density,

$$\overline{n}_e(r,z',t'') = \frac{1}{4\pi}\int_0^{2\pi}\int_0^\pi n_e(r,z',t'',\theta,\chi)\sin\theta d\theta d\chi,$$
(5)

and $\overline{x}(r,z',t'')$ is the orientation-averaged induced dipole moment,

$$\overline{x}(r,z',t'') = \widehat{F}^{-1}[\overline{x}(r,z',\omega)],$$
(6)

with $\widehat{F}^{-1}$ being the inverse Fourier transform operator and

$$\overline{x}(r,z',\omega) = \frac{1}{4\pi}\int_0^{2\pi}\int_0^\pi x(r,z',\omega,\theta,\chi)\sin\theta d\theta d\chi.$$
(7)

The detailed derivation of these equations can be found in Ref. [55], including the definition of spatial and time parameters in different frames. Here $x(r,z',\omega,\theta,\chi)$ can be obtained from the QRS theory. We follow Ref. [55] where the molecular phase and geometric phase are separated [see Eq. (3)]. The nonlinear polarizations at the frequency ω are calculated for a batch of laser peak intensities and then stored. The nonlinear polarizations for molecules inside the medium during the propagation are obtained by interpolation, and the geometric phase is then added up. For each frequency ω, Eq. (1) is solved using the Crank-Nicholson method (see Ref. [55]).

Once the harmonic field on the exit face of the gas jet ($z' = z_{out}$) is obtained, the harmonic spectra can be determined by integrating over the transverse plane:

$$S_h(\omega) \propto \int_0^\infty |\widetilde{E}_h(r,z_{out},\omega)|^2 2\pi r dr.$$
(8)

Note that harmonic yields calculated here are the total signal emitted from the gas jet. If a slit is used to select the harmonic emission, then we have to specify the region to collect the harmonics in the far field. This has been addressed in Ref. [56].

B. Response of single nonlinear polyatomic molecule to an intense laser field

1. Strong-field approximation

For a linearly polarized laser pulse, the parallel component of the induced dipole moment using the SFA can be expressed as

$$x(t) = i\int_0^\infty d\tau \left(\frac{\pi}{\epsilon + i\tau/2}\right)^{3/2} [\sin\theta\cos\chi d_x^*(t)$$
$$+ \sin\theta\sin\chi d_y^*(t) + \cos\theta d_z^*(t)][\sin\theta\cos\chi d_x(t-\tau)$$
$$+ \sin\theta\sin\chi d_y(t-\tau) + \cos\theta d_z(t-\tau)]E(t-\tau)$$
$$\times \exp[-iS_{st}(t,\tau)]a^*(t)a(t-\tau) + \text{c.c.},$$
(9)

where $d_x(t)$, $d_y(t)$, and $d_z(t)$ are the x, y, and z components of the transition dipole moment between the ground state and the continuum state. This is the generalization of the SFA from the original model of Lewenstein *et al.* [39] for molecular targets; see Refs. [40,41]. In the SFA, the continuum state is approximated by a plane wave. $E(t)$ is the electric field of the laser pulse, and ϵ is a positive regularization constant. We use (X, Y, Z) and (x, y, z) to label the laboratory fixed frame and the molecular frame, respectively. Note that θ is the angle between the Z and z axes, and χ denotes a rotation around the z axis. The quasiclassical action at the stationary points τ is written as

$$S_{st}(t,\tau) = \int_{t-\tau}^t \left(\frac{[p_{st}(t,\tau) + A(t')]^2}{2} + I_p\right)dt',$$
(10)

where I_p is the ionization potential of the molecule and $A(t)$ is the vector potential. The canonical momentum at the stationary points is given by

$$p_{st}(t,\tau) = -\frac{1}{\tau}\int_{t-\tau}^t dt' A(t').$$
(11)

In Eq. (9), the ground-state amplitude is

$$a(t) = \exp\left[-\frac{1}{2}\int_{-\infty}^{t} w(\tau)d\tau\right], \qquad (12)$$

with the ionization rate $w(\tau)$ obtained from the molecular Ammosov-Delone-Krainov (MO-ADK) theory [59–61]. In the present simulation, the ground-state electronic wave function of H_2O is obtained from the GAUSSIAN package [62].

2. The QRS theory

The details of the QRS theory for atoms and linear molecules have been given in Ref. [48]. In this paper, we extend the QRS theory to nonlinear polyatomic molecules. According to the QRS, the induced dipole moment of nonlinear polyatomic molecules can be expressed as

$$x^{\mathrm{QRS}}(\omega,\theta,\chi) = W^{\mathrm{SFA}}(E,\theta,\chi)d(\omega,\theta,\chi), \qquad (13)$$

where the returning electronic wave packet (a complex amplitude) is obtained from the SFA and $d(\omega,\theta,\chi)$ is the "exact" transition dipole, or the recombination matrix element. The latter has been obtained from molecular photoionization codes; here we use the iterative Schwinger variational method [48,53,54,63]. In this equation, E is the electron energy, which is related to photon energy ω by $E = \omega - I_p$, where I_p is the ionization energy of the molecule. The wave packets can be obtained from

$$W^{\mathrm{SFA}}(E,\theta,\chi) = \sqrt{N(\theta,\chi)}W^{\mathrm{SFA}}(E). \qquad (14)$$

Here $N(\theta,\chi)$ is the ionization probability. It depends on the orientation angle of the molecule and is calculated from the MO-ADK [61] theory. The shape of the wave packet, i.e., the dependence of the wave packet on the electron energy, is independent on the orientation angles θ and χ; thus, the orientation-independent wave packets can be calculated at given orientation angles θ' and χ' from

$$W^{\mathrm{SFA}}(E) = \frac{1}{\sqrt{N(\theta',\chi')}}\frac{x^{\mathrm{SFA}}(\omega,\theta',\chi')}{d^{\mathrm{PWA}}(\omega,\theta',\chi')}, \qquad (15)$$

where $x^{\mathrm{SFA}}(\omega,\theta',\chi')$ is the induced dipole moment obtained from the SFA and $d^{\mathrm{PWA}}(\omega,\theta',\chi')$ is the transition dipole based on the plane-wave approximation (PWA). To save computational time, we can use Eq. (15) to calculate the orientation-independent wave packet $W^{\mathrm{SFA}}(E)$ only once. The wave packets for any other orientation angles are then obtained from Eq. (14). Note that orientation-dependent ionization probabilities in Eq. (14) could also be determined by other theoretical models, such as the SFA [64] or the TDDFT [65].

Using Eqs. (14) and (15), the laser-induced dipole moment of a nonlinear molecule within the QRS is calculated from Eq. (13), where transition dipole amplitudes are obtained from established photoionization codes [53,54,63]. Thus, with the QRS theory, major computational effort is for $d(\omega,\theta,\chi)$. However, these amplitudes need to be calculated only once for a range of photon energies. For a different laser intensity, only the wave packet $W^{\mathrm{SFA}}(E,\theta,\chi)$ has to be calculated again. However, the wave packet can be calculated from SFA. Actually, the induced dipole from SFA is only calculated for one orientation once. Thus, with QRS, the calculation of

laser-induced dipoles for hundreds of peak intensities needed for the propagation calculation is rather simple.

The separable approximation given in Eq. (13) can also be applied to laser-induced dipoles calculated using the SFA as well. This is done by replacing the transition dipole in Eq. (13) by the one where the continuum wave function is approximated by a plane wave. We call this approach the factorized SFA. This method is much faster than the standard SFA. For polyatomic molecular targets, even the standard SFA calculations would be rather time-consuming since induced dipoles have to be calculated for hundreds of orientation angles and for hundreds of laser intensities if macroscopic propagation effect is to be considered. We comment that the factorized SFA can be used to investigate the orientation dependence of HHG on the symmetry of the molecular orbitals. Previous studies have shown that the alignment dependence of HHG yields reflects the symmetry of the molecular orbitals for linear molecules. This is expected to be true for nonlinear polyatomic molecules as well if HHG is generated from a dominant molecular orbital only. On the other hand, QRS is needed to obtain more accurate HHG spectra.

III. RESULTS AND DISCUSSION

A. Differential photoionization cross sections and orientation dependence

To obtain the laser-induced dipole [see Eq. (13)] for each molecule at a fixed orientation (θ, χ), we first obtain the transition dipole $d(\omega,\theta,\chi)$ of H_2O using the well-tested photoionization code [53,54]. The wave packet is calculated following Eq. (14), where the orientation dependence of the tunneling ionization rate $N(\theta,\chi)$ is calculated from the molecular tunneling ionization theory.

Figures 1(a) and 1(b) show the orientation dependence of the differential PICSs of H_2O calculated using "molecular" code and the simple plane wave approximation, respectively. The data are for photon energy of 30 eV and for photoelectrons ejected along the polarization direction of the laser. Here we refer to "molecular" for calculations using the molecular photoionization codes [53,54]. We point out that in SFA the continuum wave function is described by a plane wave, which does not account for the structure of the molecule. In QRS, or the molecular calculation, the interaction of the continuum electron with the molecular ion core has been carefully included; thus, the properties of the polyatomic molecules are properly accounted for. Despite these these two different descriptions for the continuum wave functions, for H_2O, we can clearly see that the shapes of orientation dependence of the molecular and the PWA cross sections are quite similar except that the peak positions of the molecular one are slightly shifted to larger θ. [Their major differences will be in the dependence on the photon energy; see Fig. 1(d).]

To understand the orientation dependence of PICSs, a contour plot of the highest occupied molecular orbital (HOMO) of H_2O is shown in Fig. 1(c). Since the HOMO orbital of H_2O contains a nodal plane (i.e., yz plane) [see Fig. 1(c)], the electron cannot be easily removed if the polarization direction of the laser's electric field lies on the nodal plane. Indeed, at $\chi = 90°(270°)$, the differential PICSs are close
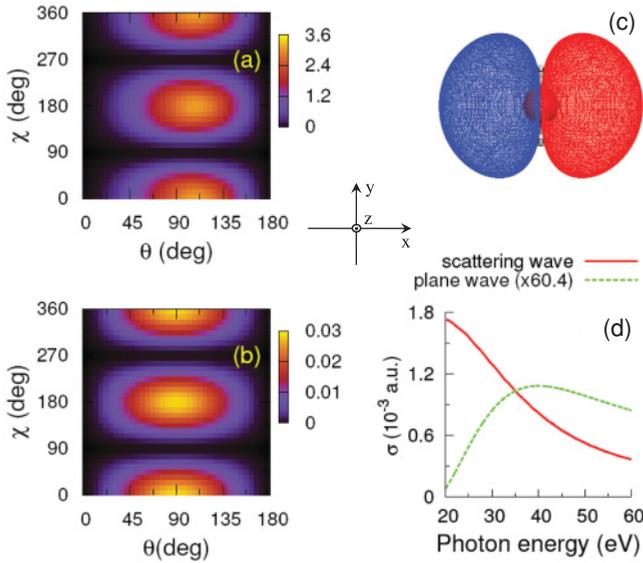
FIG. 1. (Color online) Orientation dependence of differential PICSs for H_2O obtained (a) using accurate scattering wave functions for the continuum electrons and (b) within the PWA. (c) The isointensity contour plot of the HOMO for H_2O. The sign of the HOMO wave function is indicated by different colors, i.e., red (light shading) a for positive sign and blue (dark shading) for a negative sign. (d) Comparison of the orientation-averaged differential PICSs labeled by σ for H_2O. The solid line is obtained by using scattering waves, and the dashed line is from the PWA. The x, y, and z axes of the body-fixed frame are also shown.

to zero; see Figs. 1(a) and 1(b). This result shows that the orientation dependence of PICSs (as well as the HHG), to a large extent, depends on the symmetry of the ground-state wave function of the molecule. For HHG, such dependence can be understood based on the SFA model. On the other hand, the dependence of PICS on photon energy is very sensitive to the description of continuum wave functions. Figure 1(d) shows the orientation-averaged differential PICSs of H_2O. The molecular cross section decreases monotonically as photon energy increases, while the PWA cross section first increases and then drops with the increase of photon energy, as shown in Fig. 1(d). The differences in PICSs shown in Fig. 1(d) underscore the difference of HHG predicted using the SFA vs the QRS.

B. The validity of the Factorized SFA model

Earlier, we introduced the factorized SFA model and explained that it would simplify the SFA calculations significantly. Here we demonstrate the accuracy of HHG spectra obtained from the factorized SFA. Figure 2 compares single-molecule HHG spectra of randomly oriented H_2O from the factorized SFA with that from the standard SFA. We use a 25-fs (full width at half maximum, FWHM) laser pulse with a peak intensity of 0.6×10^{14} W/cm^2 and a central wavelength of 1200 nm. One can see that the two calculations agree very well. Thus, in this paper, all the SFA calculations are referred to calculations using the factorized SFA model. One can use the factorized SFA to explain some properties of HHG from
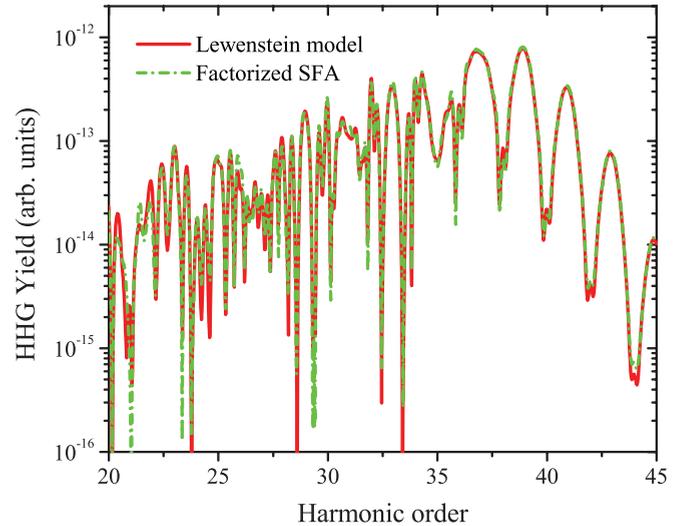

FIG. 2. (Color online) High-order-harmonic spectra calculated for individual randomly oriented H_2O molecules. Calculations using the standard SFA (or Lewenstein model) are compared to the simpler factorized SFA model.

polyatomic molecules. We show that this is true even after macroscopic propagation has been taken into account.

C. Comparison of HHG between the SFA model and the QRS

Figure 3(a) shows single-molecule HHG spectra of randomly oriented H_2O exposed to a 25-fs (FWHM) laser pulse with a peak intensity of 0.6×10^{14} W/cm^2 and a central wavelength of 1200 nm. The spectra from the SFA are normalized to that from the QRS near the cutoff. We can see that the HHG spectra from the SFA agree well with those from the QRS in the cutoff region, while there are large discrepancies in the lower plateau region. Due to the interference of long and short trajectories, the HHG spectra in the plateau region are very irregular. Clean odd harmonics can only be seen in the cutoff region. This is typical of HHG spectra from a single atom or molecule. Clean HHG spectra with sharp features require phase matching from harmonics propagated in the medium.

To obtain HHG spectra that can be compared to experiments, the laser parameters and focusing conditions have to be specified. Without such data for comparison, we consider a prototype case. In the propagation calculation, we take the fundamental IR field in space to be a Gaussian beam. The beam waist at the laser focus is fixed at $w_0 = 30 \mu m$. A 1-mm-long gas jet is placed either before, at, or after the laser focus. In the time domain, the laser pulse has a Gaussian envelope, and the carrier envelope phase is set at 0 rad. Typically, we use 300 grid points along the transverse direction and 400 grid points along the longitudinal direction in the calculation.

In Fig. 3(b), we show the calculated macroscopic HHG spectra of isotropically distributed H_2O when the gas jet is placed at 2 mm after the focus. The laser peak intensity at the center of the gas jet is 0.6×10^{14} W/cm^2. The laser wavelength and pulse duration are the same as in Fig. 3(a). Again, the macroscopic HHG spectra from the SFA are normalized to those from the QRS in the cutoff region. After propagation,
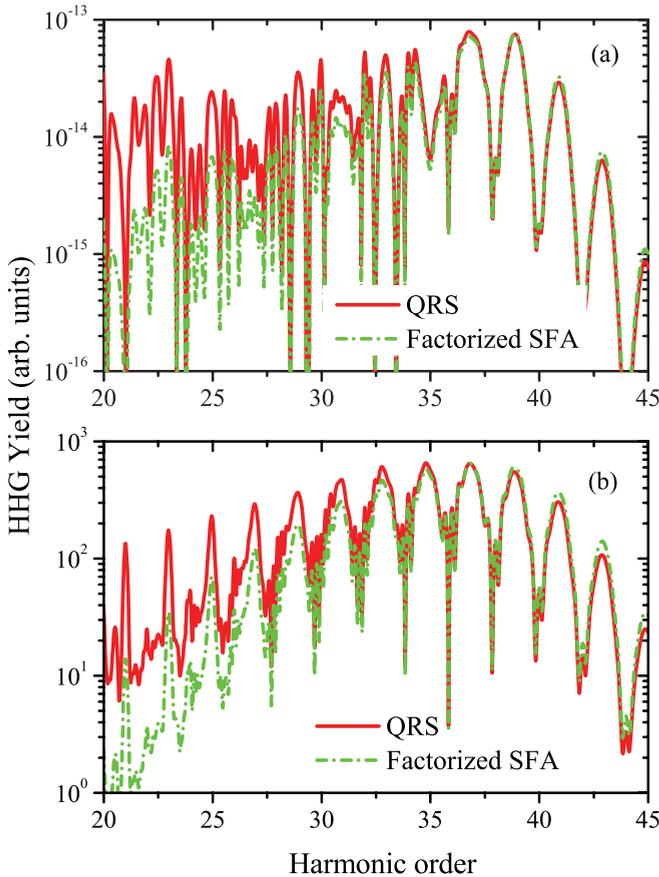
FIG. 3. (Color online) HHG spectra calculated for (a) a single H_2O molecule and (b) a macroscopic gas-phase H_2O medium including the propagation effect. Molecules are isotropically distributed.
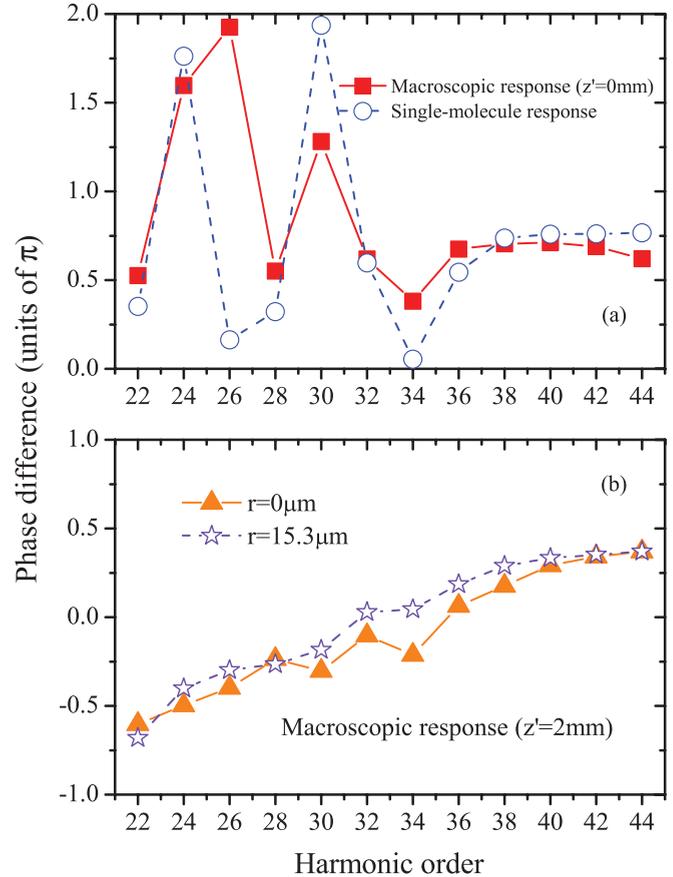

FIG. 4. (Color online) (a) Phase difference $\Delta\phi$ between successive odd harmonics for the single-molecule response (open circles) and the response after macroscopic propagation for $r = 0$ μm (solid squares). The gas jet is at the laser focus ($z' = 0$ mm). (b) Phase difference of successive order harmonics after macroscopic propagation for $r = 0$ μm (solid triangles) and for $r = 15.3$ μm (open stars). The gas jet is at 2 mm after the laser focus ($z' = 2$ mm). Molecules are randomly oriented. Laser parameters are the same as in Fig. 3.

well-resolved odd harmonics can be observed in the whole plateau region. It also shows that propagation does not reduce the discrepancies between the SFA and the QRS in the plateau region.

D. Examination of the phases of the harmonics

It is well known that phase-locked harmonics can be used to generate attosecond pulses [7–13]. According to semiclassical theory, the harmonic emission time can be determined using the phase difference between successive odd harmonics [8]. The phase differences are defined by [55]

$$\Delta\phi_{2n} = \phi_{2n+1} - \phi_{2n-1}. \tag{16}$$

In Fig. 4, we show the phase difference (note that the difference is calculated at the even harmonics) of the single-molecule response and the response after macroscopic propagation for randomly oriented H_2O. For the single-molecule response, the phase difference is defined in the interval $[0,2\pi]$. The phase difference is very irregular in the plateau region, while in the cutoff region the phases are locked well, as shown in Fig. 4(a). In Fig. 4(a), the phase difference after macroscopic propagation is also shown for a gas jet placed at the focus for harmonics measured at $r = 0$ μm. This focusing condition is known for poor phase matching, and the result shows that even after propagation, the phase difference still changes

substantially as harmonic order increases. These harmonics are not favorable for generating attosecond pulses.

Figure 4(b) shows the phase difference of the HHG after macroscopic propagation if the gas jet is placed 2 mm after the laser focus for harmonics measured at two different positions, $r = 0$ μm and $r = 15.3$ μm. In Fig. 4(b), the phase difference is shown in the interval $[-\pi, \pi]$. One can clearly see the phase difference is quite regular and increases almost linearly with the harmonic order (i.e., a linear chirp; see Ref. [8]), with the same slope for $r = 0$ μm and $r = 15.3$ μm. We comment that the slope of the phase difference for 1200-nm lasers is smaller than that for 800-nm lasers [55], in agreement with the semiclassical simulations [66].

To illustrate that phase matching is, indeed, quite complex during the propagation, in Fig. 5 we show how the harmonic intensities $|\widetilde{E}_h(r,z',\omega)|^2$ (normalized at the peak) change in space for harmonic 25 (H25), H27, H35, and H37 generated by isotropically distributed H_2O. It shows clearly that phase-matching conditions are quite different for different harmonics as the harmonics propagate in the medium. Such distributions
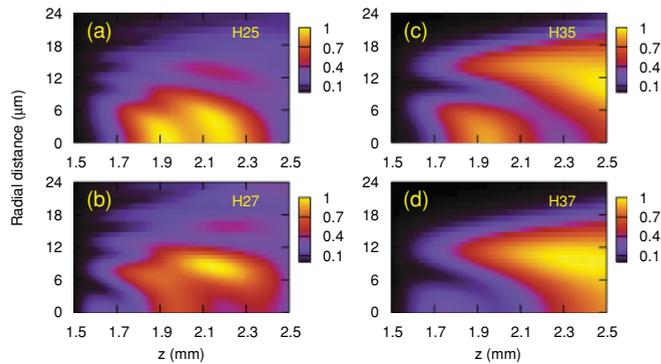
FIG. 5. (Color online) Spatial distributions of the harmonics as they propagate in the medium. (a) H25, (b) H27, (c) H35, and (d) H37. Laser parameters are the same as in Fig. 3(b).

demonstrate that an accurate quantitative comparison between theoretical calculations and experimental measurements has to be carried out under conditions as closely as possible, i.e., the experimental conditions should be carefully characterized.

IV. CONCLUSIONS

In this paper we extend the QRS theory to study high-order-harmonic generation from isotropically distributed nonlinear polyatomic gaseous H_2O molecules. We include the macroscopic propagation effect under the condition that the gas density is low and the laser intensity is not too high, such that the medium is not severely ionized [55]. The fundamental IR field is assumed to be a Gaussian beam, and the macroscopic HHG

are obtained by solving Maxwell's equation for the harmonics. We calculate the induced dipole from each molecule using the quantitative rescattering theory developed recently. The induced nonlinear polarization is then used to generate HHG in the medium. The QRS plays an essential role here since it uses accurate photorecombination transition dipoles obtained from the state-of-the-art codes in molecular photoionization theory (photoionization and photorecombination are inverse processes with respect to each other), and it also provides a simple method for calculating induced dipole moments from molecules at different orientations and peak intensities. The latter are needed in the solution of the propagation equation. We study how the magnitude and the phase of each harmonic are affected by the position of the gas jet with respect to the laser focus. Further experimental studies of HHG from nonlinear polyatomic molecules, especially for molecules that are aligned or oriented, will be of great interest.

[1] T. Brabec and F. Krausz, Rev. Mod. Phys. **72**, 545 (2000).
[2] F. Krausz and M. Ivanov, Rev. Mod. Phys. **81**, 163 (2009).
[3] C. D. Lin, A.-T. Le, Z. Chen, T. Morishita, and R. R. Lucchese, J. Phys. B **43**, 122001 (2010).
[4] M. Lein, J. Phys. B **40**, R135 (2007).
[5] A. Rundquist *et al.*, Science **280**, 1412 (1998).
[6] R. A. Bartels *et al.*, Science **297**, 376 (2002).
[7] P. M. Paul *et al.*, Science **292**, 1689 (2001).
[8] Y. Mairesse *et al.*, Science **302**, 1540 (2003).
[9] M. Hentschel *et al.*, Nature (London) **414**, 509 (2001).
[10] R. Kienberger *et al.*, Nature (London) **427**, 817 (2004).
[11] G. Sansone *et al.*, Science **314**, 443 (2006).
[12] E. Goulielmakis *et al.*, Science **320**, 1614 (2008).
[13] H. Mashiko, S. Gilbertson, C. Li, S. D. Khan, M. M. Shakya, E. Moon, and Z. Chang, Phys. Rev. Lett. **100**, 103906 (2008).
[14] S. Baker, J. S. Robinson, C. A. Haworth, H. Teng, R. A. Smith, C. C. Chirilă, M. Lein, J. W. G. Tisch, and J. P. Marangos, Science **312**, 424 (2006).
[15] W. Li, X. Zhou, R. Lock, S. Patchkovskii, A. Stolow, H. C. Kapteyn, and M. M. Murnane, Science **322**, 1207 (2008).
[16] N. L. Wagner, A. Wüest, I. P. Christov, T. Popmintchev, X. Zhou, M. M. Murnane, and H. C. Kapteyn, Proc. Natl. Acad. Sci. USA **103**, 13279 (2006).
[17] C. Altucci *et al.*, Phys. Rev. A **73**, 043411 (2006).
[18] R. Torres *et al.*, Phys. Rev. Lett. **98**, 203007 (2007).

[19] R. A. Ganeev, L. B. Elouga Bom, J. Abdul-Hadi, M. C. H. Wong, J. -P. Brichta, V. R. Bhardwaj, and T. Ozaki, Phys. Rev. Lett. **102**, 013903 (2009).
[20] M. C. H. Wong, J.-P. Brichta, and V. R. Bhardwaj, Phys. Rev. A **81**, 061402(R) (2010).
[21] M. C. H. Wong, J.-P. Brichta, and V. R. Bhardwaj, Opt. Lett. **35**, 1947 (2010).
[22] G. P. Zhang, Phys. Rev. Lett. **95**, 047401 (2005).
[23] C. B. Madsen and L. B. Madsen, Phys. Rev. A **76**, 043419 (2007).
[24] M. F. Ciappina, A. Becker, and A. Jaroń-Becker, Phys. Rev. A **76**, 063406 (2007).
[25] P. V. Redkin and R. A. Ganeev, Phys. Rev. A **81**, 063825 (2010).
[26] M. Falge, V. Engel, and M. Lein, Phys. Rev. A **81**, 023412 (2010).
[27] C. B. Madsen, M. Abu-samha, and L. B. Madsen, Phys. Rev. A **81**, 043413 (2010).
[28] E. Priori *et al.*, Phys. Rev. A **61**, 063801 (2000).
[29] C. Jin, H. J. Wörner, V. Tosa, A.-T. Le, J. B. Bertrand, R. R. Lucchese, P. B. Corkum, D. M. Villeneuve, and C. D. Lin, e-print arXiv:1012.1892.
[30] M. B. Gaarde, J. L. Tate, and K. J. Schafer, J. Phys. B **41**, 132001 (2008).
[31] P. B. Corkum, Phys. Rev. Lett. **71**, 1994 (1993).

[32] J. L. Krause, K. J. Schafer, and K. C. Kulander, Phys. Rev. Lett. **68**, 3535 (1992).

[33] M. Lein, N. Hay, R. Velotta, J. P. Marangos, and P. L. Knight, Phys. Rev. Lett. **88**, 183903 (2002).

[34] G. L. Kamta and A. D. Bandrauk, Phys. Rev. A **71**, 053407 (2005).

[35] D. A. Telnov and Shih I. Chu, Phys. Rev. A **76**, 043412 (2007).

[36] X. B. Bian and A. D. Bandrauk, Phys. Rev. Lett. **105**, 093903 (2010).

[37] X. Chu and Shih I. Chu, Phys. Rev. A **63**, 023411 (2001).

[38] D. A. Telnov and Shih I. Chu, Phys. Rev. A **80**, 043412 (2009).

[39] M. Lewenstein, Ph. Balcou, M. Yu. Ivanov, A. L'Huillier, and P. B. Corkum, Phys. Rev. A **49**, 2117 (1994).

[40] X. X. Zhou, X. M. Tong, Z. X. Zhao, and C. D. Lin, Phys. Rev. A **71**, 061801(R) (2005).

[41] X. X. Zhou, X. M. Tong, Z. X. Zhao, and C. D. Lin, Phys. Rev. A **72**, 033412 (2005).

[42] A.-T. Le, X. M. Tong, and C. D. Lin, Phys. Rev. A **73**, 041402(R) (2006).

[43] S. Odžak and D. B. Milošević, Phys. Rev. A **79**, 023414 (2009).

[44] A. Abdurrouf and F. H. M. Faisal, Phys. Rev. A **79**, 023405 (2009).

[45] C. C. Chirilă and M. Lein, Phys. Rev. A **73**, 023410 (2006).

[46] T. Morishita, A.-T. Le, Z. Chen, and C. D. Lin, Phys. Rev. Lett. **100**, 013903 (2008).

[47] A.-T. Le, R. R. Lucchese, M. T. Lee, and C. D. Lin, Phys. Rev. Lett. **102**, 203001 (2009).

[48] A.-T. Le, R. R. Lucchese, S. Tonzani, T. Morishita, and C. D. Lin, Phys. Rev. A **80**, 013401 (2009).

[49] A.-T. Le, T. Morishita, and C. D. Lin, Phys. Rev. A **78**, 023814 (2008).

[50] A.-T. Le, R. Della Picca, P. D. Fainstein, D. A. Telnov, M. Lein, and C. D. Lin, J. Phys. B **41**, 081002 (2008).

[51] A.-T. Le, R. R. Lucchese, and C. D. Lin, J. Phys. B **42**, 211001 (2009).

[52] A.-T. Le, R. R. Lucchese, and C. D. Lin, Phys. Rev. A **82**, 023814 (2010).

[53] F. A. Gianturco, R. R. Lucchese, and N. Sanna, J. Chem. Phys. **100**, 6464 (1994).

[54] A. P. P. Natalense and R. R. Lucchese, J. Chem. Phys. **111**, 5344 (1999).

[55] C. Jin, A.-T. Le, and C. D. Lin, Phys. Rev. A **79**, 053413 (2009).

[56] C. Jin, A.-T. Le, and C. D. Lin, Phys. Rev. A **83**, 023411 (2011).

[57] V. Tosa, H. T. Kim, I. J. Kim, and C. H. Nam, Phys. Rev. A **71**, 063807 (2005).

[58] M. B. Gaarde, M. Murakami, and R. Kienberger, Phys. Rev. A **74**, 053401 (2006).

[59] X. M. Tong, Z. X. Zhao, and C. D. Lin, Phys. Rev. A **66**, 033402 (2002).

[60] S.-F. Zhao, C. Jin, A.-T. Le, T. F. Jiang, and C. D. Lin, Phys. Rev. A **81**, 033423 (2010).

[61] S.-F. Zhao, J. Xu, C. Jin, A.-T. Le, and C. D. Lin, J. Phys. B **44**, 035601 (2011).

[62] M. F. Frisch *et al.*, GAUSSIAN 03, revision B.04, Gaussian, Inc., Pittsburgh, PA, 2003.

[63] C. Jin, A.-T. Le, S.-F. Zhao, R. R. Lucchese, and C. D. Lin, Phys. Rev. A **81**, 033421 (2010).

[64] T. K. Kjeldsen, C. Z. Bisgaard, L. B. Madsen, and H. Stapelfeldt, Phys. Rev. A **68**, 063407 (2003).

[65] S. K. Son and Shih I. Chu, Chem. Phys. **366**, 91 (2009).

[66] G. Doumy, J. Wheeler, C. Roedig, R. Chirla, P. Agostini, and L. F. DiMauro, Phys. Rev. Lett. **102**, 093002 (2009).